BULLETIN OF THE POLISH ACADEMY OF SCIENCES
TECHNICAL SCIENCES, Vol. 69(6), 2021, Article number: e138821
DOI: 10.24425/bpasts.2021.138821

Wind tunnel tests of hovering propellers in the transition state of Quad-Plane

Katarzyna POBIKROWSKA and Tomasz GOETZENDORF-GRABOWSKI*

Institute of Aeronautics and Applied Mechanics, Warsaw University of Technology, ul. Nowowiejska 24, 00-665 Warsaw, Poland

Abstract. The following paper presents wind tunnel investigation of aerodynamic characteristics of hovering propellers. This propulsion system may be applied on a lightweight Quad Plane VTOL (Vertical Take-Off and Landing) UAV (Unmanned Aerial Vehicle). A Quad Plane is a configuration consisting of a quadcopter design combined with a conventional twin-boom airplane. This kind of design should therefore incorporate the advantages of both types of vehicles in terms of agility and long endurance. However, those benefits may come with a cost of worse performance and higher energy consumption. The characteristics of a fixed-wing aircraft and propellers in axial inflow are well documented, less attention is put to non-axial flow cases. VTOL propellers of a hybrid UAV are subject to a multitude of conditions – various inflow speeds and angles, changing RPMs, interference between propellers and between nearby aerodynamic structures. The tested system presented in this article consists of four electric motors with two coaxial pairs of propellers mounted on one of the fuselage beams. Such a configuration is often chosen by designers of small and medium hybrid UAVs. There is a need for studies of clean, efficient ways of transporting, and this article can aid future designers of a new type of electric UAVs.

Key words: wind tunnel; propeller; VTOL; hybrid UAV; aerodynamics; propulsion.

1. INTRODUCTION

Currently, the most often used UAVs in class up to 25 kg are the multicopters. The ability of vertical take-off and landing is the fundamental advantage of such vehicles. The significant problem of multicopters is their relatively small speed and limited range due to batteries' capacity. A good solution are the hybrid UAVs that combine the VTOL and horizontal capabilities in one vehicle. Such vehicles are generally called the Transitional Aircraft (TA) in that they require the addition of a transition phase between the hovering mode and the fixed-wing mode. The most important features of this configuration are increased range, endurance, altitude, payload carrying capacity, and maximum forward speed compared to typical rotorcraft [1]. A survey of such vehicles presented by Saeed *et al.* in [2], shows rapidly growing popularity of hybrid UAV and probable domination of such configuration on the market. Moreover, many different configurations are considered by designers [3].

One of the promising configurations is a Quad Plane which is powered by eight counter-rotating hovering propellers in coaxial pairs and one pushing propeller (Fig. 1). This configuration was selected for the design of new unmanned medium and long-range aircraft enabling the transport of cargo or measuring equipment [4]. One of the key problems is the transition from vertical to horizontal flight, i.e., from a copter to a classic fixed wing flight. The copter flight is very energy consuming because all lift force is generated by eight propellers driven by

Fig. 1. Quad Plane configuration

electric motors, therefore this phase's duration should be reduced to the minimum required [5, 6]. It differs from the classic airplane configuration, where the energy needed to take off is much lower [7]. Propellers used on VTOL aircraft are always subjected to various air inflow angles, varying from axial inflow during the take-off and landing phases to non-axial during transition and horizontal flight. This is in opposition to helicopters and propeller-powered fixed-wing airplanes in which the range of angles the propeller operates in is limited ($80^\circ - 90^\circ$ for helicopters and $0^\circ - 10^\circ$ for fixed-wing aircraft) [8]. Most of the research on propellers considers the case of inflow normal to the propeller plane [9–11], and very little work is focused on the full angle of attack range. In the transition phase, all copter propellers work in almost tangential flow and aerodynamic characteristics [12] in such a case are less known. Cerny [13] also points to the fact, that the majority of propellers used on VTOL aircraft are designed only for the axial inflow case. There were some attempts at establishing the propeller characteristics for non-axial inflow conditions for both limited and full (0° to 180°) propeller angle of attack range that are presented in paper [13] and in NACA/NASA reports [14–17]. While it can be assumed that for the tangential inflow, the lift

*e-mail: tgrab@meil.pw.edu.pl

Manuscript submitted 2021-06-01, revised 2021-07-19, initially accepted for publication 2021-08-15, published in October 2021

force will not change significantly, the aerodynamic drag during transition flight may be large, which will result in extending the acceleration time of the aircraft to the minimum speed for horizontal flight. However, on the other hand, the copter propellers thrust component in the airspeed direction can support forward thrust in case of negative incidence angle. The theoretical analysis based on blade element theory (BET) allowed to estimate the effect of tangential flow on propellers thrust, torque and necessary power [18]. BET theory is mainly used for analyzing helicopter rotors [19] however, its idea was first suggested by Drzewiecki [20] for aircraft propeller analysis. A similar problem was investigated by Foster and Hartman [21], however they focused on much more complex goal, i.e., "high fidelity simulation of quadrotor" and their results are not conveniently applicable in each case. Therefore, to study the characteristics of propellers in a parallel flow to their plane, a wind tunnel test program was implemented [22], which resulted in lift and drag coefficients as a function of angle of attack and flow velocity. Moreover, the necessary power was tested as a function of the airspeed. The results of experimental studies were compared with the results of theoretical considerations. The obtained results allowed proper estimation of the capacity of the batteries supplying motors for vertical flight and the necessary thrust generated by the marching propulsion unit.

Different VTOL aircraft have different scenarios for the transition from hovering to level flight. The modelling of quadrotor flight and control is well presented in [23]. Much attention has to be put into proper design of the transition phase. The requirements that this phase has to fulfil are: minimal transition time, minimal altitude loss and minimal energy consumption [1]. In case of the class of the fixed engines/fixed wing VTOL aircraft the transition scenario is simple: using the hovering propellers start the climb until you reach transition altitude. Then, start the pushing propeller and keep accelerating until a required airspeed is achieved at which point the thrust force of hovering engines is replaced by lift force from the wings. During this time slowly reduce the hovering propellers' thrust to keep the altitude constant. In the presented work a different profile of transition is considered – possibility to use the hovering propellers to aid the acceleration of level flight. This can be done by placing the whole aircraft at the suitable pitch angle and utilizing the projection of thrust force in the flight direction, all the while keeping the aircraft at a constant altitude. The results of presented research can be valuable for modifying the control in transition to shorten this phase of flight and to size such a vehicle [24].

2. THEORETICAL CONSIDERATIONS

Theoretical considerations contain two aspects. First the necessary power as a function of airspeed referred to the static thrust condition was examined. Secondly, the aerodynamic drag of rotating propellers and possible forward thrust increment were estimated.

Airflow normal to the propeller plane causes the following effects: an increase of lift with airflow flowing from below the propeller (as shown in Fig. 2) or a decrease of lift with airflow from above the propeller (as shown in Fig. 3). The angle of attack of the blade section and therefore the propeller's lift is linked with the tail-boom's angle of attack and the propeller's rotational velocity. As for the airflow tangential to the propeller's plane, it causes an increase of lift on the advancing blade and a decrease on the retreating blade (shown in Fig. 4 and 5). High non-axial inflow angles introduce periodic effects that influence propeller thrust [13]. However, when using a coaxial counter-rotating pair, the overall result is that both propellers lift force increases with increasing airflow. Negative effects (such as lift asymmetry or undesirable pitch and yaw moments) are present for each propeller but reduced for the combined pair. In the figures, the angle of attack α is the propeller blade section's angle of attack (not to be mistaken with the tail-boom angle of attack, used further in the presented work).

Taking notation in Figs. 4 and 5, the lift dL and drag dD per unit span on the blade element are:

$$dL = \frac{1}{2}\rho V_R^2 c C_l dr, \qquad dD = \frac{1}{2}\rho V_R^2 c C_d dr, \tag{1}$$

where: c – blade chord, C_l – blade section lift coefficient, C_d – blade section drag coefficient, ρ – air density. The contributions to thrust, torque and power of the propeller blade are as follows

$$\begin{aligned} dT &= dL\cos\phi - dD\sin\phi, \\ dQ &= (dL\sin\phi - dD\cos\phi)r, \\ dP &= (dL\sin\phi - dD\cos\phi)\omega r, \\ \phi &= \beta - \alpha, \end{aligned} \tag{2}$$

where: β – propeller pitch angle, α – angle of attack, ω – engine angular velocity, r – radial position of propeller section. The induced angle ϕ is small or even equal to zero in tangential airflow case, so we can assume that $\sin\phi = \phi = 0$ and $\cos\phi = 1$, therefore equations above result in:

$$\begin{aligned} dT &= dL - \phi dD, \\ dQ &= (\phi dL - dD)r, \\ dP &= (\phi dL - dD)\omega r. \end{aligned} \tag{3}$$

The resultant propeller section airflow velocity V_R is the vector sum of the airflow due to the free stream and angular rate of propeller. In case of tangential free stream and pure advancing and retreating blade (azimuth ± 90 deg) the V_R is simply scalar sum or difference of V_T (tangential airflow) and ωr (Fig. 4 and 5). Therefore, the lift dL and drag dD contributions have the form:

$$dL = \frac{1}{2}\rho(\omega r \pm V_T)^2 c C_l dr, \quad dD = \frac{1}{2}\rho(\omega r \pm V_T)^2 c C_d dr \tag{4}$$

To simplify calculation, we assumed that blade chord is constant versus radius (it is often strictly true in case of helicopter rotor) and the blade is untwisted. While V_N (normal airflow) is equal to zero also lift and drag coefficient can be assumed as

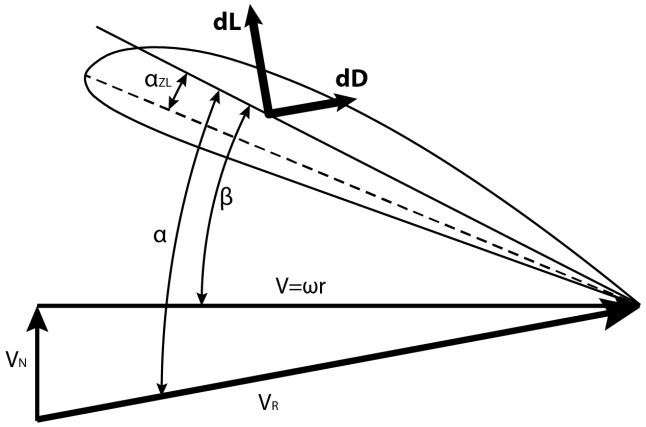

Fig. 2. airflow normal from below the propeller

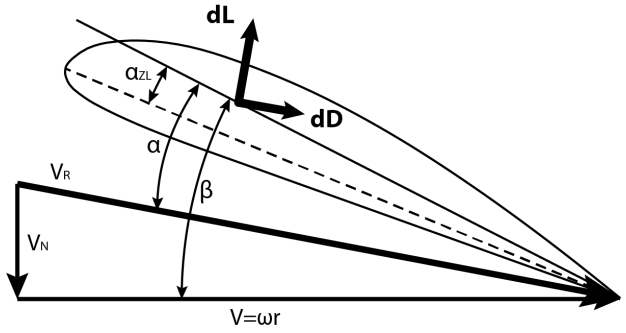

Fig. 3. airflow normal from above the propeller

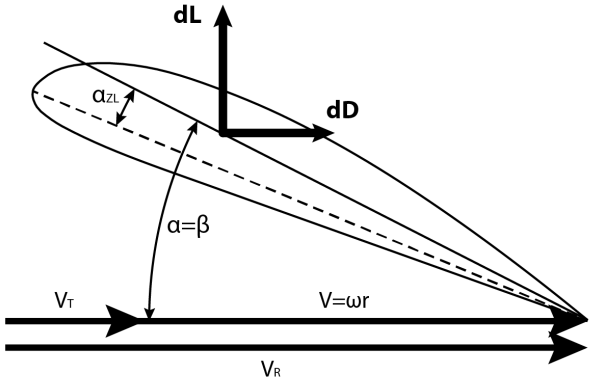

Fig. 4. airflow tangential (advancing blade)

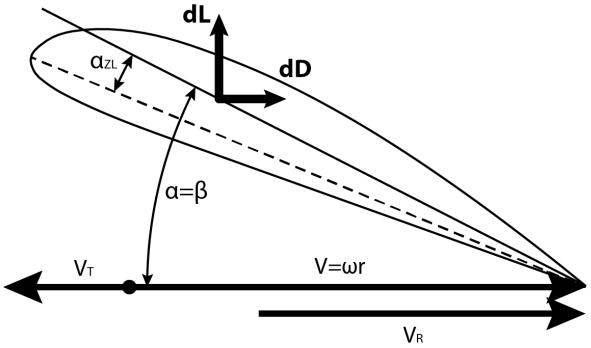

Fig. 5. airflow tangential (retreating blade)

constant versus radius. Integrating equation (3) with respect to radius and taking into account relations (4), we obtain:

$$\begin{aligned} T = L &= \int_0^R \frac{1}{2}\rho(\omega r \pm V_T)^2 c C_l \,\mathrm{d}r = \\ &= \frac{\rho}{2} c R C_l \left(\frac{\omega^2 R^2}{3} \pm \omega V_T R + V_T^2\right), \\ P &= \int_0^R \frac{1}{2}\rho(\omega r \pm V_T)^2 c C_d \omega r \,\mathrm{d}r = \\ &= \frac{\rho}{2} c R C_d \omega \left(\frac{\omega^2 R^3}{4} \pm \frac{2}{3}\omega V_T R^2 + \frac{1}{2} V_T^2 R\right). \end{aligned} \tag{5}$$

For a two-blade propeller, as the one analyzed in the paper, in one moment in time two propeller blades – advancing and retreating, generate thrust and power as shown in equation (6) – a sum of two blades.

$$\begin{aligned} T_{\text{total}} &= \rho c R C_l \left(\frac{\omega^2 R^2}{3} + V_T^2\right), \\ P_{\text{total}} &= \rho c R C_d \omega \left(\frac{\omega^2 R^3}{4} + \frac{1}{2} V_T^2 R\right). \end{aligned} \tag{6}$$

Let $T_{\text{total},0}$, $P_{\text{total},0}$ and ω_0 be the required thrust, power and angular velocity for the case of no airflow (V_T=0). To calculate thrust gain from increased airflow, assuming a small change in angular velocity it can be written:

$$\frac{T_{\text{total}}}{T_{\text{total},0}} = \frac{\omega^2 R^2 + 3V_T^2}{\omega_0^2 R^2} = \left(\frac{\omega}{\omega_0}\right)^2 + \frac{3V_T^2}{\omega_0^2 R^2} = 1 + \frac{3V_T^2}{\omega_0^2 R^2}. \tag{7}$$

As can be seen from equation (7), thrust slightly increases versus air speed.

Referring to equation (3), the power required by the propeller is a function of angular velocity. During the tunnel tests presented in this paper, the thrust value was set to a constant value for all the considered air speeds. To ensure the constant thrust (i.e., $T_{\text{total}} = T_{\text{total},0}$), the engines' angular velocity had to be changed.

Assuming the approximated model presented in this section, the change in angular velocity can be written as:

$$\omega = \sqrt{-\frac{3V_T^2}{R^2} + \omega_0^2 \frac{T_{\text{total}}}{T_{\text{total},0}}} = \sqrt{\frac{3V_T^2}{R^2} + \omega_0^2}. \tag{8}$$

Equation (8) clearly shows a decrease of the angular velocity (to preserve constant thrust) as air speed increases. Combin-

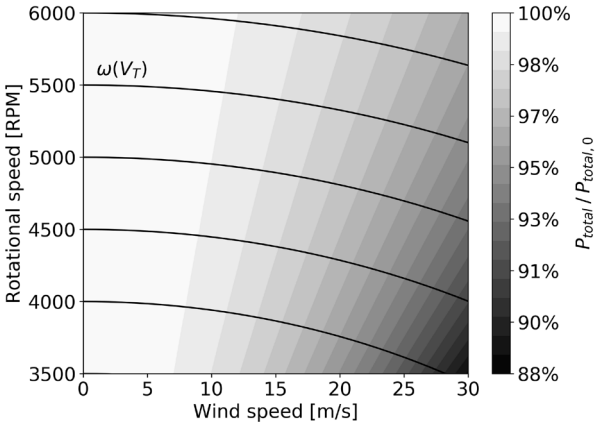

Fig. 6. contour plot showing relation between the decrease in required power, the engines' rotational speed and air speed

ing equation (8) and power equation (6) and plotting $\frac{P_{\text{total}}}{P_{\text{total},0}}$ as a function of ω_0 and V_T, Fig. 6 can be obtained. It shows the change of required power with air speed and rotational speed. Here, R is assumed as the radius of the analyzed propeller, which is 9.5 inches. From the figure it can be concluded that for larger air speeds, smaller power is needed for propulsion. This effect is more pronounced for smaller rotational speeds.

It's important to note here, that this result could only be used in a qualitative way, and not quantitative. Its purpose here is to show a general trend because of all the adopted simplifications.

Coaxial propellers are usually combined in counter rotating pairs to eliminate their torque and to lower or even completely eliminate tangential slipstream velocity loss [25]. Moreover, propellers placed in coaxial pairs are claimed to be more efficient than conventional single propellers. This is due to a reduction of the rotational motion of the fluid, thus reducing the momentum loss. The coaxial pair also has an ability to obtain maximum thrust without the high Mach tip speed losses. On the other hand, coaxial propellers generate more noise, which can be lowered by differentiating of rotational speed between the two propellers [26]. The efficiency of the coaxial propeller pair is largely influenced by their mutual induced flow and by the flow around the beam between them [27, 28]. These effects decrease propellers' installed thrust. The latter effect influences the flow velocity closest to the hub of both upper and lower coaxial propellers and is called the "blockage effect". The magnitude of efficiency loss is proportional to the ratio of the blocking body section area and the propeller area. The smaller the beam area between propellers – the better the efficiency of the pair. The same can be said about the shape of the blocking body – streamlining the shape brings a higher efficiency [29].

Next important thing for the coaxial propeller pair is the distance between the propellers. Results from Bell [30] showed that the distance between propellers in a coaxial pair played a significant role in the magnitude of thrust provided by the pair. For the analyzed case of a SUAV (Small UAV), the most advantageous was the H/D (distance to diameter) ratio of 41–65%. As for the distance of propellers placed in the same plane (as is the case of the front and aft propellers of the analyzed Quadplane), the closer the propellers are, the less thrust they produce. This effect however is only pronounced for a distance smaller than one propeller diameter [31]. Important here is the fact that this conclusion is only valid for the static and the axial inflow case. For the non-axial case, front propellers obstruct the flow acting as a blocking body, and their induced flow is being pushed toward the aft propellers.

3. TEST STAND IDEA

The tested model was a tail-beam of a 25 kg VTOL airplane powered by eight counter-rotating hovering propellers in coaxial pairs and one pushing propeller (Fig. 7). Eight propellers

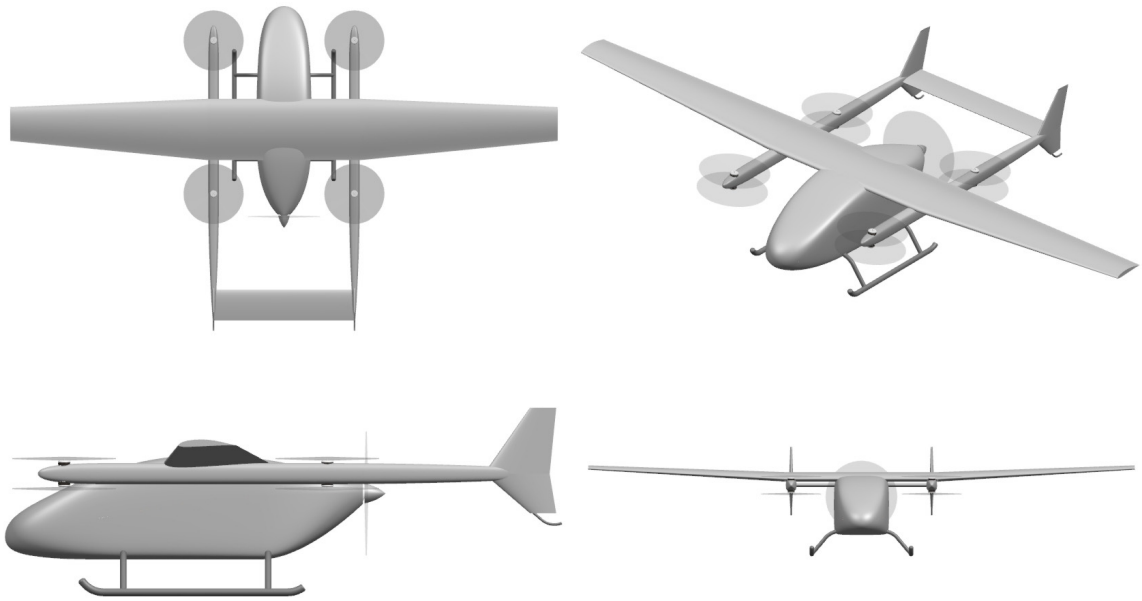

Fig. 7. UAV in Quad Plane configuration

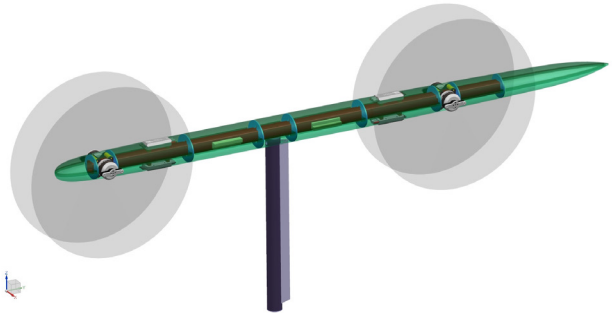

Fig. 8. Tail-beam with four propellers mounted on the mast

must provide enough thrust to enable ascending, hovering and transition of the aircraft. The aircraft is equipped with two tail-beams that hold four propellers each. Due to the symmetry of the model in the tunnel tests only one of the two tail-beams and 4 of 8 propellers were considered. Therefore, all calculations are based on half of the weight of the aircraft (12.5 kg).

The test stand consisted of the beam mounted on a mast, which separates the beam with propellers from the wind tunnel table (Fig. 8). Because the measurement system was installed at the bottom of the mast in the wind tunnel table, measured values (forces and moments of forces) had to be recalculated.

Three coordinate systems (Fig. 9) have been defined to allow the analysis and presentation of the results. The convention for numbering the motors is also shown in the figure: 3rd and 4th motors are the front motors, and 1st and 2nd are the rear motors. The convention is used throughout the rest of the article.

First coordinate system, named "scale", is related to the mast base, and is directly linked with the strain gauges system. The data from the sensors is provided in this axis system. The second coordinate system is a body axis system (similar to body axis system defined for flight dynamic analysis): origin of the system is located in equal distance from front and rear motors (point B), X_b is directed forward (to the beam front), Z_b is in the contradict direction to the propellers' thrust and Y_b according to the right-hand rule (downward). The third coordinate system named "aerodynamic" axis system is the body axis system rotated by angle of attack about Y axis.

To properly interpret the data coming from the strain gauge scales, it was necessary to calculate forces and moments of forces in body and aerodynamic axis systems. Analysis below shows the transition from scales' forces in its axis system to other systems starting with the "body" axis system. Equation (9) presents the moment of forces after translation of the origin from point "0" to point "B"

$$\vec{M}_B = \vec{M}_0 + \vec{r}_b \times \vec{F} \tag{9}$$

The moment of forces components are as follows:

$$\begin{aligned} \vec{M}_B = [M_x, M_y, M_z] + [0,0,-r] \times [F_X, F_Y, F_Z] = \\ = [M_x + rF_Y, M_y - rF_X, M_z] \end{aligned} \tag{10}$$

where r is the distance between "0" and "B" points and is equal to 0.5 meters. The next step is the rotation of the axis system

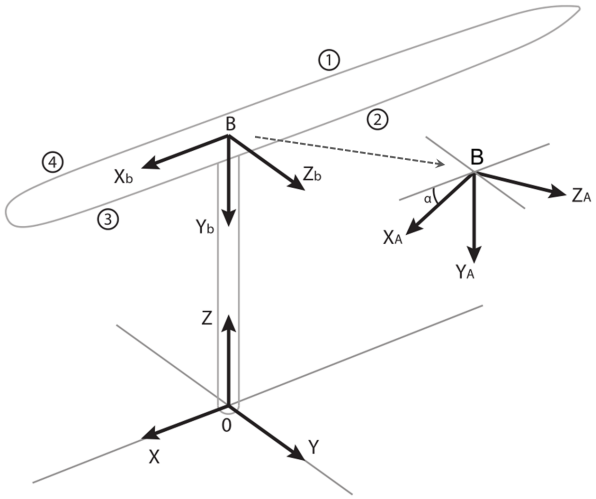

Fig. 9. The coordinate systems used for analysis

by 90 degrees around X axis, which gives the transformation in the following form:

$$\begin{bmatrix} Fx_b \\ Fy_b \\ Fz_b \\ Mx_b \\ My_b \\ Mz_b \end{bmatrix} = \begin{bmatrix} 1 & 0 & 0 & 0 & 0 & 0 \\ 0 & 0 & -1 & 0 & 0 & 0 \\ 0 & 1 & 0 & 0 & 0 & 0 \\ 0 & 0 & 0 & 1 & 0 & 0 \\ 0 & 0 & 0 & 0 & 0 & -1 \\ 0 & 0 & 0 & 0 & 1 & 0 \end{bmatrix} \begin{bmatrix} 1 & 0 & 0 & 0 & 0 & 0 \\ 0 & 1 & 0 & 0 & 0 & 0 \\ 0 & 0 & 1 & 0 & 0 & 0 \\ 0 & r & 0 & 1 & 0 & 0 \\ -r & 0 & 0 & 0 & 1 & 0 \\ 0 & 0 & 0 & 0 & 0 & 1 \end{bmatrix} = \begin{bmatrix} Fx \\ Fy \\ Fz \\ Mx \\ My \\ Mz \end{bmatrix} \tag{11}$$

The primary source of the F_{bz} force is the thrust of the propellers. The F_{bx} force is a "drag" of the tail-beam and propellers. The pitching moment (M_{by}) with respect to the Y_b-axis is caused by thrust difference between front and rear propellers (1,2 and 3,4 pairs). The final transformation from the body to aerodynamic axis system is presented by equation (12).

$$\begin{bmatrix} Fx_A \\ Fy_A \\ Fz_A \\ Mx_A \\ My_A \\ Mz_A \end{bmatrix} = \begin{bmatrix} \cos\alpha & 0 & \sin\alpha & 0 & 0 & 0 \\ 0 & 1 & 0 & 0 & 0 & 0 \\ -\sin\alpha & 0 & \cos\alpha & 0 & 0 & 0 \\ 0 & 0 & 0 & \cos\alpha & 0 & \sin\alpha \\ 0 & 0 & 0 & 0 & 1 & 0 \\ 0 & 0 & 0 & -\sin\alpha & 0 & \cos\alpha \end{bmatrix} \begin{bmatrix} Fx_b \\ Fy_b \\ Fz_b \\ Mx_b \\ My_b \\ Mz_b \end{bmatrix} \tag{12}$$

Within the wind tunnel test it had to be examined if the eight hovering propellers could provide the necessary thrust and how much of the horizontal force could be gained to reinforce thrust of a marching propulsion unit. The scheme of forces from two pairs of propellers is presented in Fig. 10. It shows one of two tail-beams at an angle to the flow (for simplification, the angle of attack in the tunnel is the same as the pitch angle). The F_{bx} and F_{bz} forces are the resultant propulsion and thrust forces of four propellers. The transformation from body to the aerodynamic coordinate system rewritten from matrix form (12) to simplify equations, shows equation (13).

$$\begin{aligned} F_{ax} &= F_{bx}\cos\alpha + F_{bz}\sin\alpha\,, \\ F_{az} &= F_{bz}\cos\alpha - F_{bx}\sin\alpha\,. \end{aligned} \tag{13}$$

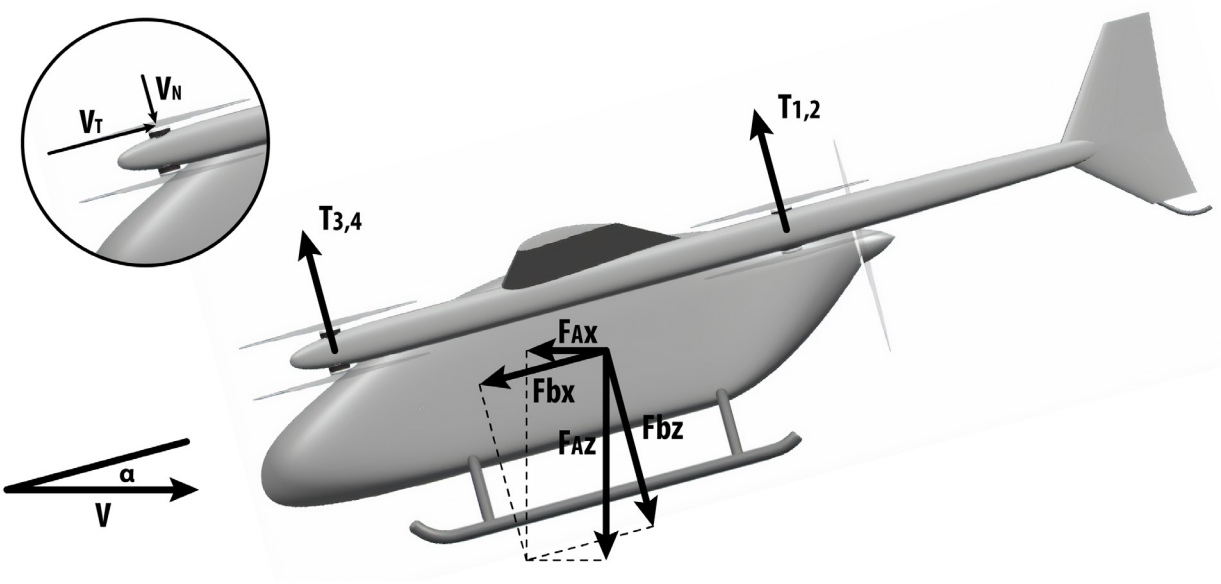

Fig. 10. Propulsion forces at an angle of attack

Tunnel tests were performed for 4 KDE4215XF-465 brushless electric motors. Its parameters are listed in Table 1.

Batteries used in tests were five 6S LiPo batteries that provided 12Ah each and maximum voltage of 25.2 V. They had to be charged every 30 minutes to ensure sufficient voltage and proper operation of the engines. Engines were controlled using PWM (pulse-width modulation). Each engine was equipped with current and voltage sensors.

The experimental research was carried out in the closed-loop wind tunnel with an adjustable turbulence level, located at the Institute of Aeronautics and Applied Mechanics of the Warsaw University of Technology. The technical parameters of the tunnel and test section are as follows:

- the cross section size: 2.5 m × 2.0 m,
- the working area length: 10 m,
- airspeed range: 5–25 m/s,
- the power of turbine: 250 kW.

Force measurements (forces and moments in all three axes) were collected with a tensometric scales. The rotating table to which the scales was mounted, allowed for a full 360 degrees rotation. Other tunnel sensors included: Pitot tube to measure air speed, temperature sensor, humidity sensor. Table 2 shows the tensometric scales' force limits.

Table 1
KDE4215XF-465 electric motor specifications

Kv	Voltage Range	Maximum Power	Maximum Current
465 RPM/V	14.8-26.1 V	1375 W (180 s)	62 A (180 s)

Table 2
Force limits of strain gauge scales

Fx [N]	Fy [N]	Fz [N]	Mx [Nm]	My [Nm]	Mz [Nm]
2000	2000	2000	200	200	50

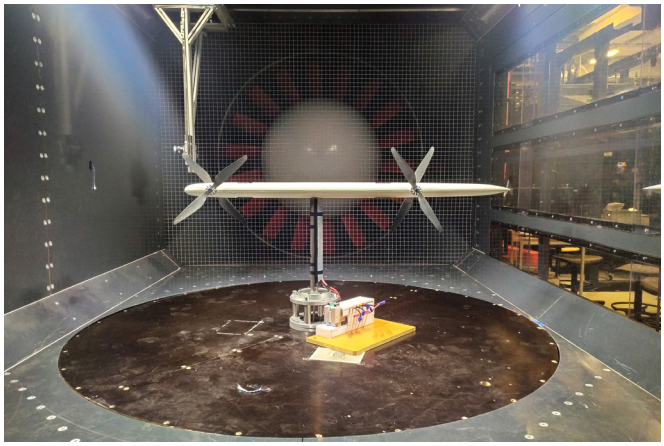

Fig. 11. Tail-boom in the aerodynamic tunnel

4. WIND TUNNEL TEST PROGRAM

The tests were conducted for a fixed pitch propeller (19″ × 5.7″), for two air speeds (10 and 20 m/s). These speeds are in the proximity of the analyzed aircraft's stall speed and flight speed, and hence were chosen for testing. The primary goal of the tests was to investigate the effect of air speed and angle of attack on the forces generated by and on the propellers. The following parameters were investigated: static thrust, dynamic thrust for two air speeds (4 engines running) and dynamic thrust for two air speeds (3 of 4 engines running – simulated dysfunction of each of the engines). The dynamic thrust tests were performed in the equilibrium state i.e., for the angle of attack 0, the Fbz force equal to the weight of the aircraft for various cases of desired lift force and the Mby moment equal to 0. Summary of the test program is shown in Fig. 12. The weight cases analyzed here (lower than 100%) were chosen to keep the load to a minimum to prevent the engines from overheating and overworking. Attempts at increasing the thrust above 100% in high

velocity and angle of attack ranges resulted in engine and propeller damage. The 100% weight case represented hover of the aircraft.

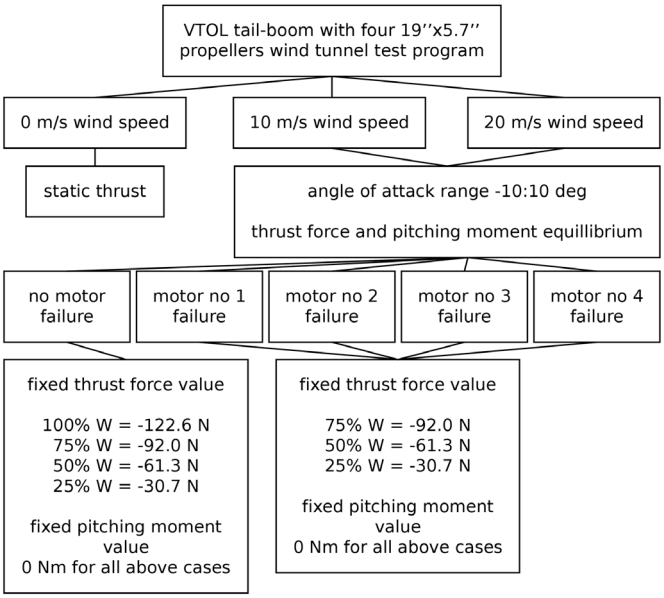

Fig. 12. Wind tunnel test program

The first challenge was to establish engines PWM values to maintain equilibrium state. For simplification, it was assumed that engines operated in pairs i.e., two front engines shared the same PWM value as well as the aft pair (for the state of no simulated engine failure). Because of no generic PWM to force relation in the airflow was available, those equilibrium state PWM values had to be determined experimentally for each air speed (10 and 20 m/s) and each of 5 experiment cases (with and without engine failure). From the available data from the static measurements outside the tunnel of the relation between thrust force and PWM values could not be concluded the same in the wind flow. First obvious reason for that is the change in propellers' characteristics in presence of airflow. Another reason is the high interference between coaxial propellers (for the static tests only one propeller was used). These effects are very difficult (if possible at all) to predict analytically. The PWM to force relations were aqcuired for the case of AoA=0 so that it was possible later to find the characteristics with changing angle of attack.

This was done as follows: measurements were collected for PWM values of 20%, 40%, 60%, 80% for all combinations. Although such choice of the data points may seem too sparse, after collecting and interpolating the results they proved to be sufficiently accurate and the method not too time consuming. An example of the relations $F_{bz}(\mathrm{PWM_{front}}, \mathrm{PWM_{rear}})$ and $M_{by}(\mathrm{PWM_{front}}, \mathrm{PWM_{rear}})$ is shown in Fig. 13. On the picture "12" means rear engines, while "4" means front engines. This engine numbering convention is shown in Fig. 9. In the contour plot, solid grey lines symbolize lines of constant thrust force (in black: lines of thrust force of 25%, 50%, 75% and 100% of aircraft weight). Grey dashed lines symbolize lines of constant pitching moment (in black: line of zero pitching moment – equilibrium). PWM values of equilibrium (for four cases of aircraft weight) can be found where black dashed and solid lines meet. It can be seen in the figure, that thrust of larger magnitude could be obtained while keeping moment equilibrium, but as stated earlier, higher thrust cases could overload the engines and the propellers and cause damage at higher angles of attack.

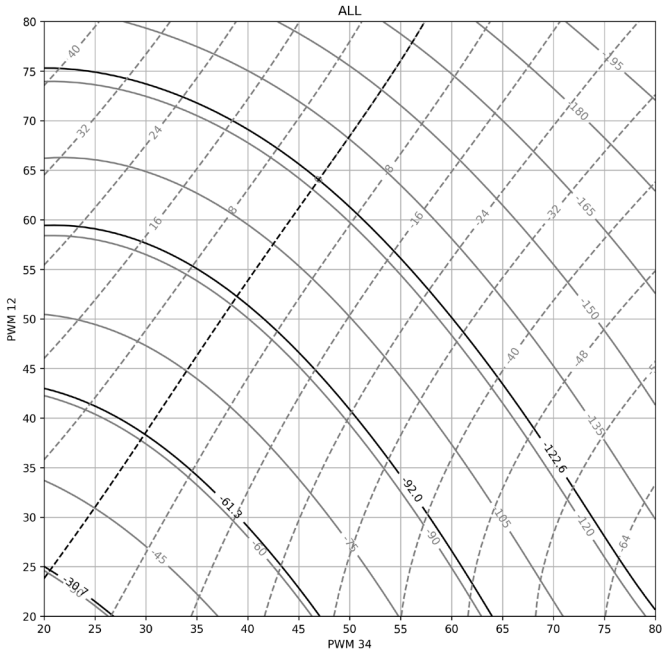

Fig. 13. Example PWM to thrust force and PWM to pitching moment relation (air speed of 20m/s, no failure case)

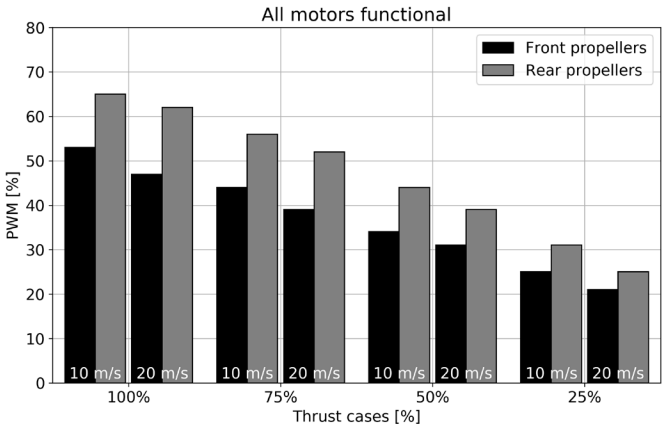

Fig. 14. PWM equilibrium values for a no-failure case (two flight speeds, four thrust cases)

Important to note here is that not for all failure cases 100% of aircraft weight was achieved. For most cases the highest value was 75% of weight. Only the no-failure case can obtain thrust of 100% of aircraft weight. This can be observed in Figs. 14 and 15.

Due to constantly changing tunnel parameters, such as temperature and humidity, the PWM to force/moment relation

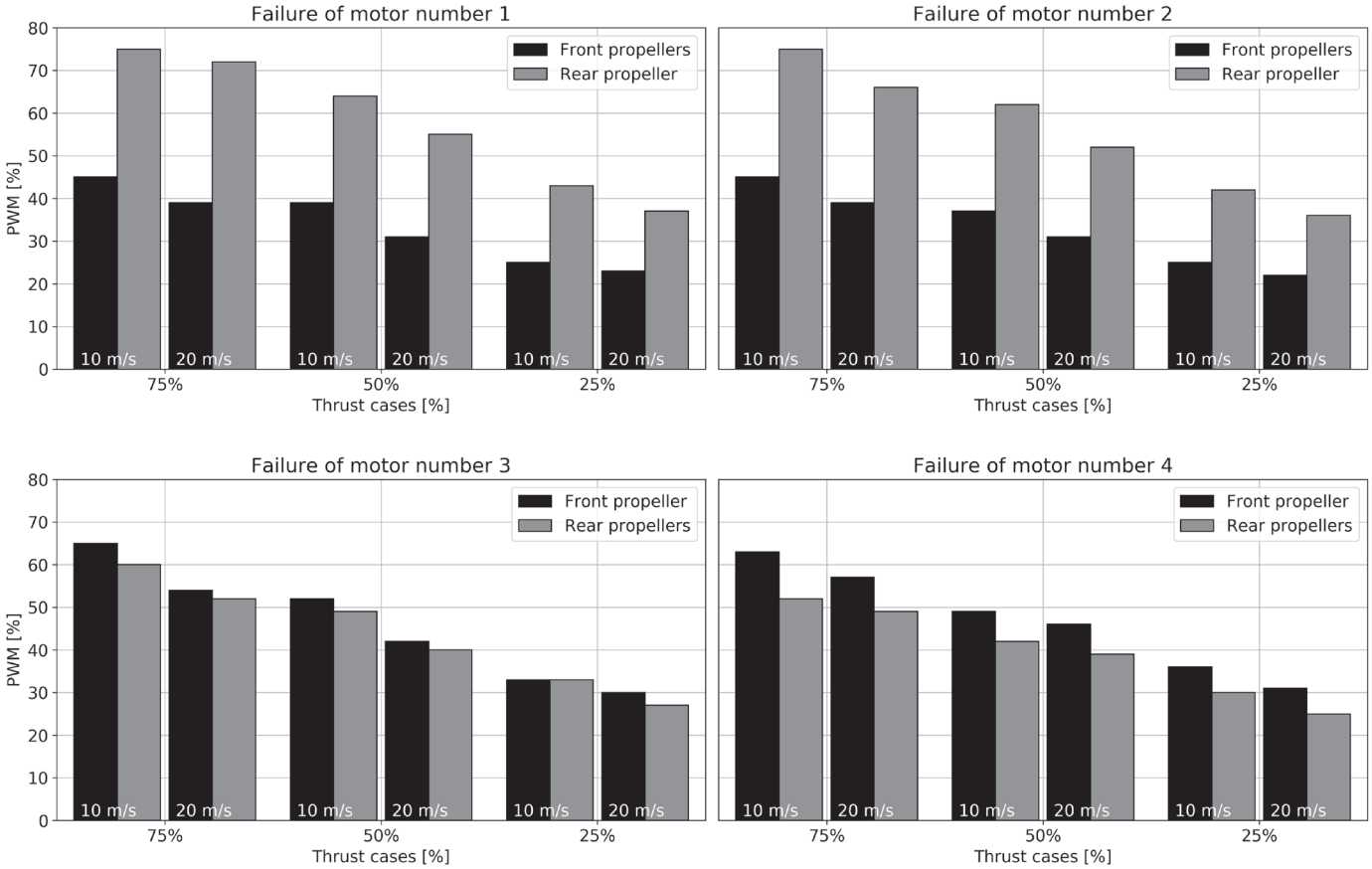

Fig. 15. PWM equilibrium values for failure cases (two flight speeds, four thrust cases)

changed. The equilibrium PWM values used in further tests had to be altered slightly by performing validation: everyday, PWM values were checked and, if necessary, changed based on how much error they gave from the equilibrium force and moment values. This change was usually very small. From this point, the presented equilibrium PWM values will be consistent throughout the next sections of this article. Figures 14 and 15 show PWM values read from PWM/force/moment plots such as the example one presented in Fig. 13 (and altered slightly where necessary).

The trend in the figures is clear – in the case of no failure, the rear motors are more loaded than the front motors despite being the same distance point B (Fig. 9). It gives a rather unsettling conclusion that the rear propellers will lower the maximum thrust of the propulsion system. The maximum thrust can be obtained by setting all motors' PWM values to the high limit, but this case would be unbalanced – the thrust with which the force and moment equilibrium is maintained is lower and limited on the rear motors and propellers. What else can be noticed in Fig. 15 is that the failure of either of the rear (first or second) propellers will result in the inability to uphold the full aircraft weight (only up to 75%).

All propellers are mounted in the same distance from the measurement sensor and in the case of no airflow equal PWM values on all motors create no moment around the Yb axis. However, it changes when the airflow is present – then with equal PWM values thrust of each propeller pair is different and creates a moment on the strain gauge scales. This is mostly due to the induced flow of the propellers being pushed backwards with the airflow. Figure 14 shows the difference in front and rear pair's PWM values. Comparing it with third and fourth (front) motor failure plot in Fig. 15, this difference is smaller, because only one front propeller generates induced flow.

With the PWM equilibrium values obtained, the main part of tests could be performed and that was to evaluate the aerodynamic characteristics i.e., in regard to the changing angle of attack. Below are listed main requirements to ensure correct results from the tunnel tests:

1) keep the battery voltage on the right level i.e., 24–25 V,
2) ensure constant tunnel environment parameters: temperature 20–30°C, humidity 30–50%,
3) avoid damaging the motors: short testing sequences to not overheat the motors, low angles of attack and airflow speeds to limit propeller load,
4) avoid overloading the strain gauge scales: limit maximum differential propellers' thrust forces.

The goal of the tunnel tests was to determine whether the chosen motors could perform the task of hovering the full mass of the aircraft in the case of no failure and one motor failure. Further goals were to find the power necessary to maintain aircraft's hover, evaluate the effect of changing air speed and angle of attack and to test a possible transition scenario.

5. WIND TUNNEL RESULTS

In this section are presented tunnel test results: static thrust and characteristics in regard to a changing angle of attack for two flight speeds. To simplify, only results for a case of all motors functioning are shown (cases of failure showed similar trend, so are omitted here). Figure 16 shows horizontal force F_{bx}, thrust force F_{bz} and pitching moment M_{by} (each for two flight speeds: 10 m/s and 20 m/s and for four cases of fixed thrust value – from 25% to 100% of aircraft weight). Key takeaways from the graphs are as follows: Fbx is constant with angle of attack and only its magnitude is variable with flight speed. The magnitude of Fbz grows linearly with angle of attack with the proportionality constant increasing with flight speed. The pitching moment M_{by} increases as angle of attack increases.

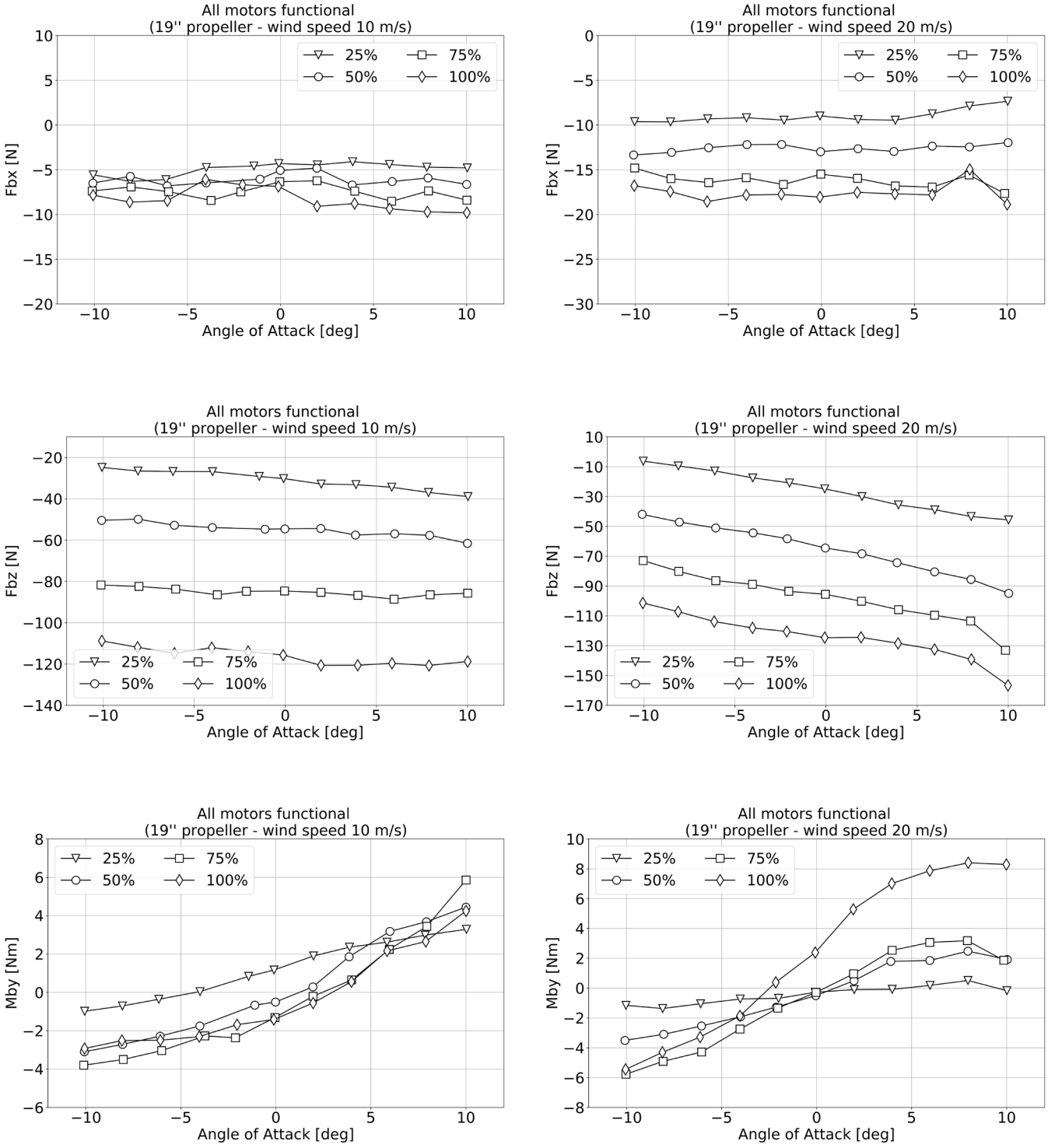

Fig. 16. tail-boom's characteristics with regard to changing angle of attack (for two airspeeds)

F_{bz} force can be thought of as the thrust of the tail-boom and the propulsion system. The reason for the increase of this force was shown in section 2. Positive angle of attack brings an increase of the air inflow from below the propeller thus increasing the thrust. The "lift" of the tail-boom and other aerodynamic effects can be omitted for being of much smaller magnitude than the propellers' thrust. As for M_{by}, its presence is due to the different flow conditions of the front and aft propeller pairs. The aft propellers operate in a more disturbed flow because of the front propellers' induced flow being pushed to the back of the tail-beam. As stated earlier, the aft propeller pair operated on higher PWM values and used more power to sustain tail-beam equilibrium. Thrust/moment to PWM maps (Fig. 13) can be used to predict if the propulsion system will be able to oppose the increasing pitching moment. As can be seen from the example map, all engines can sustain equilibrium of the pitching moment in a wide range while still providing the ability to hover.

Although the method to obtain PWM values for equilibrium was efficient and brought reliable results, it had one serious drawback – the determined PWM values were correct only for certain tunnel environment variables such as temperature and humidity which changed quite rapidly during the tests. The tunnel was equipped with devices to lower the humidity, but it took a long time to obtain the desirable value. Adding to that the strain gauge scales error, a small difference between measured value and equilibrium value is visible on characteristics in Fig. 16.

Figure 17 shows static thrust and efficiency of the tested engine and propeller. This test was performed for a single propeller, on a dynamometer outside the aerodynamic tunnel and without the tail-beam present. The maximum thrust of the propeller is about 60N for the PWM of 90% and the maximum propeller efficiency is about 75% for a PWM value of 70%.

In Fig. 18 the propeller thrust loss due to interference (static conditions) is shown. Analyzed effects were the tail-boom blockage effect and the thrust loss in coaxial propeller pair. The baseline is the single propeller shown in Fig. 17. The analysis was conducted for the PWM value of 90% (most prominent thrust loss due to interference). Most visible thrust loss was due

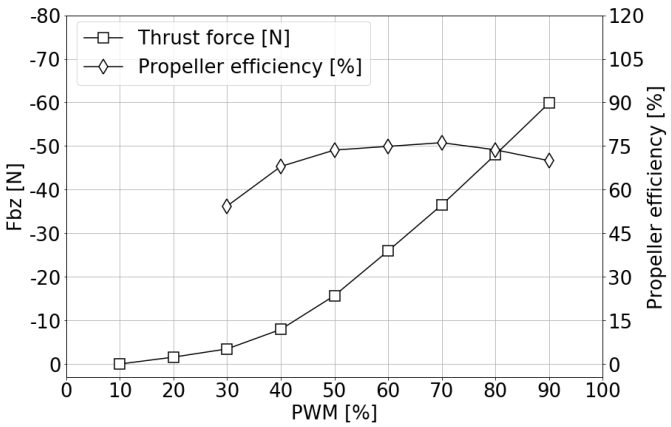

Fig. 17. $19'' \times 5.7''$ propeller static thrust and efficiency in function of PWM values

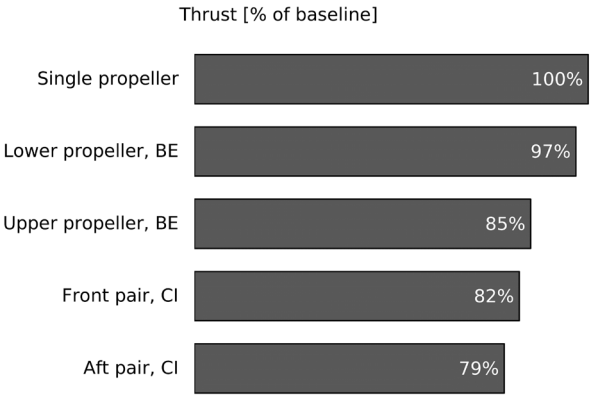

Fig. 18. Influence of the interference effects on the propeller thrust. BE – Blockage Effect, CI – Coaxial Interference

to the coaxial interference (20%), while blockage effect alone accounted for about 15% loss. As can be noticed, the least thrust was produced by the aft propeller pair (21%). This was due to both mentioned effects. The aft pair fully surrounds the blocking body, while the front pair protrudes before the tail-boom, with half of its area being in a clean, undisturbed flow (shown in Fig. 8). Failure of the upper aft engine will cause the most danger for the aircraft, while failure of lower front engine will be the safest (provide most thrust).

Figure 19 shows total electric power usage i.e., used by all working motors. This is shown for two air speeds and for the angle of attack 0 deg. As can be seen from the graph, the electric power required for sustaining the weight of the aircraft is lower as air speed increases. The reason for this was mentioned above and presented in Fig. 4. For a set value of rotational speed (and therefore PWM value) as the air speed increases, so does the thrust of the propeller pair. To acquire a thrust value of full aircraft weight for a higher air speed a lower rotational speed is needed and therefore lower power. Although the magnitude of the power decrease is larger than that shown in earlier section, the model used previously was only approximate. Nevertheless, the model correctly predicted the decrease of power consumed as air speed increased.

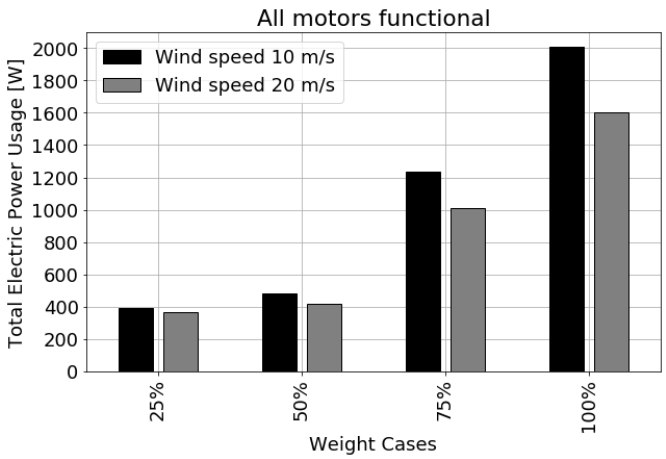

Fig. 19. Total electric power usage of all 4 motors in case of no-failure

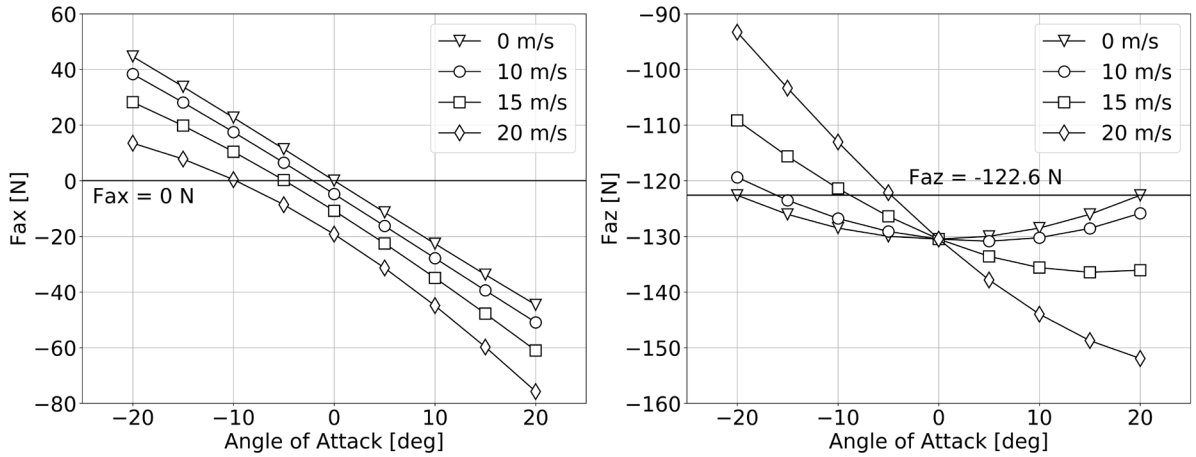

Fig. 20. Theoretical model of Fax and Faz force for various air speeds

6. WIND TUNNEL RESULTS VERSUS THEORY

From plots in Fig. 16 in Wind tunnel results the following can be concluded (this is also true for the cases of failure, not presented in this article):

1. The F_{bx} force is constant with the angle of attack. The value increases as the air speed increases. It can be estimated as shown in equation (14). This represents the equivalent drag for a streamlined body with a drag coefficient equal to 0.1 ($\rho = 1.225\ \mathrm{kg/m^3}$). Data from the wind tunnel proved the diameter of this body (d) was equal to 1 m.

$$F_{bx} = -\frac{1}{2}\rho S V^2 C_x = -\frac{1}{2}\rho \frac{\pi}{4} d^2 V^2 C_x = -0.0481 V^2. \quad (14)$$

2. The F_{bz} force increases with increasing angle of attack. The slope of the function is higher, the higher the air speed. In other words, it can be expressed as in equation (15). Data collected from the tests shows that ζ is a function of only the air speed. This function can be estimated based on data from Table 3. Note the negative sign, which is due to the chosen coordinate system Z-axis direction. Q in the equation stands for the force equilibrium values (weight percentage cases as in Fig. 12).

$$F_{bz} = Q + \zeta(V) \cdot \alpha\,. \quad (15)$$

3. The M_{by} moment increases with increasing angle of attack. This is an adverse effect that will cause the aircraft's static instability and must be corrected by the autopilot or compensated by an increase of static margin of the aircraft.

In Fig. 20 are shown F_{ax} and F_{az} forces for equilibrium value Q of -130.5 N for various air speeds. As can be seen, for angle of attack -20 deg, line of 0 m/s (hovering) the value of $F_{az} = -122.6$ N (100% aircraft weight). Reading Fax value for the same angle, we notice $F_{ax} = 42.6$ N. This is the gained horizontal force to quicken the acceleration of the aircraft (for the pitch angle of -20 deg). As the air speed increases a bigger value of Q is necessary to allow for horizontal acceleration maintaining Faz of -122.6 N.

Q in equation (15) can be considered as propellers' static thrust. Plotting similar graphs for other values of Q can be used to find a relation between pitch angle of the aircraft, loss of vertical force to sustain hover and the horizontal force gain to quicken the transition for the cases of non-zero airflow.

These considerations are valid only for one tail-beam. For the full aircraft model, they must be expanded by adding forces of the second tail-beam and the remaining aircraft components (e.g., lifting surfaces, fuselage).

Table 3
$\zeta(V)$ function

V [m/s]	0	10	20
$\zeta(V)$ [N/deg]	0.00	–0.26	–1.91

7. CONCLUSIONS

This paper presents wind tunnel investigation of coaxial contra-rotating rotor configuration used in VTOL propulsion system of the Quad Plane aircraft. Two sets of fully functioning coaxial rotors were mounted on tail-boom mock-up connected to aerodynamic 6-elements balance on turntable in the wind tunnel. Such configuration is characterized by strong coupling of aerodynamic parameters between aircraft components and propellers. The methods for quick estimation of such complex interference are still unavailable. Therefore, a simple model to describe the resultant aerodynamic forces for this particular case was created. It described two forces – the tail-boom thrust force and the horizontal force. The former depended on wind speed and angle of attack, the latter on wind speed squared. Upon this simple analysis it was possible to estimate the gained horizontal force to quicken transition to the horizontal flight. Another effect that was analyzed was the influence of high propeller angles of attack, and the changing wind speed. Theoretical considerations correctly predicted the influence of increasing the wind speed on power consumption of the propulsion system. The higher the wind speed tangential to the propeller plane, the lower the necessary power. The Quad Plane configu-

ration features many sources of aerodynamic interference, e.g., between aircraft components and propellers (blockage effect), within the coaxial propeller pair, between propellers on different axes (front and aft propellers, hover and pushing propellers) and possibly other, not mentioned here. The most prominent seems to be the coaxial interference, which caused about 20% of thrust loss in comparison to a single propeller. These effects can be lessened by narrowing and streamlining the blocking body, careful design of the coaxial configuration and by placing the hover propellers far from other aircraft components and from the pushing propeller. Conclusions impacting the usage of the aircraft and its control strategies are as follows:

1. Interference causes asymmetry of the operation of each propeller. Especially important here is the blockage effect. Because of it, rotors mounted of top of the tail-boom generate about 10% less thrust than bottom rotors. Therefore, in case of one engine failure, different emergency control strategies are needed depending on whether failure impacts top or bottom engines.
2. Coaxial rotors mounted before wing are producing more thrust due to a smaller blockage effect (tail-boom influences only the half propeller area). As a result, tail coaxial rotors have less thrust capacity, limiting aircraft's pitching moment recovery potential.
3. Quad Plane configuration proves full redundancy (in its ability to sustain hover) for any one of the front rotors' failure, and limited redundancy (controlled crush landing) for aft rotors as a consequence of their smaller thrust.
4. The proposed transition scenario of the Quad Plane was proved to be applicable.
5. Drag force produced by working VTOL propulsion system is independent of the angle of attack and increases with the wind velocity.
6. Due to relatively high Thrust to Weight ratio of VTOL propulsion system, excess power can be utilized for acceleration support of pusher motor in transition state. Wind tunnel measurements proves that VTOL system can be balanced in terms of vertical forces and moments up to minus 10 deg. angle of attack.

Conducted research showed that simplified analytical methods need to be verified experimentally especially for such complex configurations. Presented observations demonstrate complicated aerodynamic characteristics of tail-boom mounted VTOL propulsion system, without influence of the wing during transition phase. Its complexity only shows the necessity of further investigation, which is planned in next phase – wind tunnel tests of the full aircraft half-model.

ACKNOWLEDGEMENTS

The publication is supported by Project No.: POIR.01.01.01-00-0814/17 entitled: "Design and construction of unmanned medium and long-range aircraft enabling the transport of cargo or measuring equipment." This Project is being realized in cooperation with the Spectre Solutions Sp. z o.o. company and is co-financed from EU funds under the Smart Growth Operational Programme 2014–2020.

REFERENCES

[1] A.M. Kamal and A. Ramirez-Serrano, "A. Design methodology for hybrid (VTOL + Fixed Wing) unmanned aerial vehicles," *Aeronaut. Aerosp Open Access J.*, vol. 2, no. 3, pp. 165–176, 2018, doi: 10.15406/aaoaj.2018.02.00047.

[2] A.S. Saeed, A.B. Younes, C. Cai, and G. Cai, "A survey of hybrid unmanned aerial vehicles," *Prog. Aerosp. Sci.*, vol. 98, pp. 91–105, 2018, doi: 10.1016/j.paerosci.2018.03.007.

[3] A. Bacchini and E. Cestino, "Electric vtol configurations comparison," *Aerospace*, vol. 6, no. 3, 2019, doi: 10.3390/aerospace6030026.

[4] T. Goetzendorf-Grabowski, A. Tarnowski, M. Figat, J. Mieloszyk, and B. Hernik, "Lightweight unmanned aerial vehicle for emergency medical service – Synthesis of the layout," *Proc. Inst. Mech. Eng., Part G: J. Aerosp. Eng.*, vol. 235, pp. 5–21, 2020, doi: 10.1177/0954410020910584.

[5] S.D. Prior, *Optimizing Small Multi-Rotor Unmanned Aircraft*. CRC Press, Taylor & Francis Group, 2018.

[6] G. Avanzini, E.L. de Angelis, and F. Giulietti, "Optimal performance and sizing of a battery-powered aircraft," *Aerosp. Sci. Technol.*, vol. 59, pp. 132–144, 2016, doi: 10.1016/j.ast.2016.10.015.

[7] Z. Goraj, A. Frydrychewicz, R. Świtkiewicz, B. Hernik, J. Gadomski, T. Goetzendorf-Grabowski, M. Figat, S. Suchodolski, and W. Chajec, "High altitude long endurance unmanned aerial vehicle of a new generation – A design challenge for a low cost, reliable and high performance aircraft," *Bull. Pol. Acad. Sci. Tech. Sci.*, vol. 52, no. 3, pp. 173–194, 2004.

[8] D. Serrano, M. Ren, A.J. Qureshi, and S. Ghaemi, "Effect of disk angle-of-attack on aerodynamic performance of small propellers," *Aerosp. Sci. Technol.*, vol. 92, pp. 901–914, 2019, doi: 10.1016/j.ast.2019.07.022.

[9] D.G. Koenig, "V/STOL Wind Tunnel Testing," NASA Ames Research Center, Tech. Rep. TM-85936, 1984.

[10] S. Xiang, Y.-qiang Liu, G. Tong, W.-ping Zhao, S.-xi Tong, and Y.-dong Li, "An improved propeller design method for the electric aircraft," *Aerosp. Sci. Technol.*, vol. 78, pp. 488–493, 2018, doi: 10.1016/j.ast.2018.05.008.

[11] M. Rostami and A. hamzeh Farajollahi, "Aerodynamic performance of mutual interaction tandem propellers with ducted uav," *Aerosp. Sci. Technol.*, vol. 108, p. 106399, 2021, doi: 10.1016/j.ast.2020.106399.

[12] A. Bacchini, E. Cestino, B. Van Magill, and D. Verstraete, "Impact of lift propeller drag on the performance of evtol lift + cruise aircraft," *Aerosp. Sci. Technol.*, vol. 109, p. 106429, 2021, doi: 10.1016/j.ast.2020.106429.

[13] M. Cerny and C. Breitsamter, "Investigation of small-scale propellers under non-axial inflow conditions," *Aerosp. Sci. Technol.*, vol. 106, p. 106048, 2020, doi: 10.1016/j.ast.2020.106048.

[14] C.E. Hughes and J.A. Gazzaniga, "Low-Speed Wind Tunnel Performance of High-speed Counterrotation Propellers at Angleof-Attack," NASA, Tech. Rep. TM-102292, 1989.

[15] R.E. Kuhn and J.W. Draper, "Investigation of The Aerodynamic Characteristics Of A Model Wing-Propeller Combination And Of The Wing And Propeller Separately At Angles Of Attack Up To 90," NACA, Tech. Rep. 1263, 1956.

[16] H.C. McLemore and M.D. Cannon, "Aerodynamic Investigation Of A Four-Blade Propeller Operating Through An Angle-Of-Attack Range From 0 To 180," NACA, Tech. Rep. 3228, 1954.

[17] C. Russell, J. Jung, G.C. Willink, and B. Glasner, "Wind Tunnel and Hover Performance Test Results for Multicopter UAS Vehicles," NASA, Tech. Rep. TM-2018-219758, 2016.

[18] M.A.J. Kuitche, R.M. Botez, R. Viso, J.C. Maunand, and O.C. Moyao, "Blade element momentum new methodology and wind tunnel test performance evaluation for the UAS-S45 Bàlaam propeller," *CEAS Aeronaut. J.*, vol. 11, pp. 937–953, 2020, doi: 10.1007/s13272-020-00462-x.

[19] J.G. Leishman, *Principles of Helicopter Aerodynamics*, 2nd ed. Cambridge University Press, 2006.

[20] S. Drzewiecki, *Theorie Generale de l'Helice*. Paris, 1920.

[21] J.V. Foster and D. Hartman, "High-fidelity multi-rotor unmanned aircraft system (uas) simulation development for trajectory prediction under off-nominal flight dynamics," in *17th AIAA Aviation Technology, Integration, and Operations Conference*. AIAA, 2017, doi: 10.2514/6.2017-3271.

[22] K. Pobikrowska, "Wind tunnel testing of electric propulsion system for an unmanned vtol aircraft," Master's thesis,Warsaw University of Technology, 2019.

[23] R. Zawiski and M. Błachuta, "Modelling and optimal control system design for quadrotor platform – an extended approach," *Bull. Pol. Acad. Sci. Tech. Sci.*, vol. 62, no. 3, pp. 535–550, 2014, doi: 10.2478/bpasts-2014-0058.

[24] M. Tyan, N.V. Nguyen, S. Kim, and J.-W. Lee, "Comprehensive preliminary sizing/resizing method for a fixed wing – vtol electric uav," *Aerosp. Sci. Technol.*, vol. 71, pp. 30–41, 2017, doi: 10.1016/j.ast.2017.09.008.

[25] J.S. Vanderover and K.D. Visser, "Analysis of a contrarotating propeller driven transport aircraft," 2006, AIAA Student Paper Competition, Syracuse, New York, USA. 31 March–1 April.

[26] V. Štorch, M. Brada, and J. Nozicka, "Experimental setup for measurement of contra-rotating propellers," in *Proceedings Topical Problems of Fluid Mechanics 2017*, D. Šimurda and T. Bodnár, Eds., 2017, pp. 285–294, doi: 10.14311/TPFM.2017.036.

[27] C.P. Coleman, "A Survey of Theoretical and Experimental Coaxial Rotor Aerodynamic Research," NASA, Tech. Rep. TP-3675, 1997.

[28] B. Theys, G. Dimitriadis, P. Hendrick, and J. De Schutter, "Influence of propeller configuration on propulsion system efficiency of multi-rotor unmanned aerial vehicles," in *2016 International Conference on Unmanned Aircraft Systems (ICUAS)*, 2016, pp. 195–201, doi: 10.1109/ICUAS.2016.7502520.

[29] J. Roskam, *Airplane Aerodynamics and Performance*. DARcorporation, 2016.

[30] J.C. Bell *et al.*, "Development of a test-rig for exploring optimal conditions of small unmanned aerial vehicle co-axial rotor systems," in *International Conference on Manufacturing Engineering Systems*, 2010, pp. 439–444.

[31] W. Zhou, Z. Ning, H. Li, and H. Hu, "An experimental investigation on rotor-to-rotor interactions of small uav propellers," in *35th AIAA Applied Aerodynamics Conference*. AIAA, 2017, doi: 10.2514/6.2017-3744.